ELSEVIER

Journal of Crystal Growth 168 (1996) 308–323

JOURNAL OF CRYSTAL GROWTH

Ribosomal crystallography: from crystal growth to initial phasing

J. Thygesen [a], S. Krumbholz [a], I. Levin [b], A. Zaytzev-Bashan [b], J. Harms [a], H. Bartels [a], F. Schlünzen [a], H.A.S. Hansen [a], W.S. Bennett [a], N. Volkmann [a], I. Agmon [b], M. Eisenstein [b], A. Dribin [b], E. Maltz [b], I. Sagi [b,c], S. Morlang [c], M. Fua [b], F. Franceschi [c], S. Weinstein [b], N. Böddeker [c], R. Sharon [b], K. Anagnostopoulos [b,c], M. Peretz [b], M. Geva [b], Z. Berkovitch-Yellin [a,b], A. Yonath [a,b,*]

[a] *Max-Planck Unit for Structural Molecular Biology, Hamburg, Germany*
[b] *Department of Structural Biology, Weizmann Institute, Rehovot, Israel*
[c] *Max-Planck-Institute for Molecular Genetics, Berlin, Germany*

Abstract

Preliminary phases were determined by the application of the isomorphous replacement method at low and intermediate resolution for structure factor amplitudes collected from crystals of large and small ribosomal subunits from halophilic and thermophilic bacteria. Derivatization was performed with dense heavy atom clusters, either by soaking or by specific covalent binding prior to the crystallization. The resulting initial electron density maps contain features comparable in size to those expected for the corresponding particles. The packing arrangements of these maps have been compared with motifs observed by electron microscopy in positively stained thin sections of embedded three-dimensional crystals, as well as with phase sets obtained by ab-initio computations. Aimed at higher resolution phasing, procedures are being developed for multi-site binding of relatively small dense metal clusters at selected locations. Potential sites are being inserted either by mutagenesis or by chemical modifications to facilitate cluster binding to the large halophilic and the small thermophilic ribosomal subunits which yield crystals diffracting to the highest resolution obtained so far for ribosomes, 2.9 and 7.3 Å, respectively. For this purpose the surfaces of these ribosomal particles have been characterized and conditions for quantitative reversible detachment of selected ribosomal proteins have been found. The corresponding genes are being cloned, sequenced, mutated to introduce the reactive side-groups (mainly cysteines) and overexpressed.

To assist the interpretation of the anticipated electron density maps, sub-ribosomal stable complexes were isolated from H50S. One of these complexes is composed of two proteins and the other is made of a stretch of the rRNA and a protein. For exploiting the exposed parts of the surface of these complexes for heavy atom binding and for attempting the determination of their three-dimensional structure, their components are being produced genetically. The low resolution models reconstructed from tilt series of crystalline arrays of ribosomal particles are being employed for initial phasing. The tentative functional interpretation of these models stimulated the design and the crystallization of complexes mimicking

* Corresponding author. Fax: +49 40 891314; E-mail: yonath@mpgars.desy.de.

PII S0022-0248(96)00338-7

defined functional states, which were found to be of a higher quality than that obtained from crystals of isolated ribosomes. Specific binding of multi-metal clusters to these complexes is currently underway.

Keywords: Ribosomes, Crystallography of; Undecagold cluster; Heteropolyanion clusters

1. Introduction

Ribosomes provide the site for the translation of the genetic code into polypeptide chains in all living cells. They are built of two independent subunits of unequal size which associate upon the initiation of protein biosynthesis. A typical bacterial ribosome (70S) is of molecular weight of 2.3 million daltons and its large (50S) and small (30S) subunits of 1.45 and 0.85 million daltons, respectively. About one third of the ribosomal mass is comprised of up to 73 different r-proteins, depending on the source. The rest are three rRNA chains with a total of about 4500 nucleotides. To shed light on the molecular mechanisms involved in protein biosynthesis, ribosomal crystallography was initiated. The currently studied crystal systems include ribosomes and their complexes mimicking defined functional states as well as soaked, chemically modified and mutated ribosomal subunits (Table 1 [1–7]). In general, efforts are being made to keep the conditions for crystal growth as close as possible to the physiological environment of the ribosomal particles [8–10].

Despite the recent increase in sophistication of the crystallographic instrumentation and the implementation of powerful genetic techniques, the ribosomes are still considered extremely complicated for crystallographic studies. Being intracellular ribonucleoprotein organelles, known to be notoriously flexible, unstable, conformationally heterogenous, of complex structure, enormous size with no internal symmetry, even their crystallization still depends on a large number of parameters, among which rational and mystery are playing equal roles. Thus, during the course of our investigations it was shown that ribosomal crystallography may be described as an unpredictable journey, often associated with barrier crossings and sharp turning points, some of which required conceptual revisions and led to unexpected developments.

A partial list of the parameters which have been identified as influencing ribosomal crystallization is given below: the ribosomal source (bacterial type and the specific strain); the procedures used for bacterial growth (the exact composition of the growth media and its pH, the size of the fermentor, its shape, the speed of agitation); the procedures for the preparation of the ribosomes and the separation of their subunits (the centrifugation parameters, the size of the separation columns, the ribosomal concentrations); the biochemical and functional homogeneity of the preparation (for instance, no crystals could be grown from ribosomal particles with a low functional activity, but not all active preparations do); the chemical homogeneity of the preparation (e.g. the r-proteins/rRNA ratio and the extent of the integrity of the rRNA chains, as some nuclease activity is always detected even if it does not affect substan-

Table 1
Characterized three-dimensional crystals of ribosomal particles

Source	Grown form	Average cell dimensions	Resolution (Å)
T70S[1]	MPD [a]	$524 \times 524 \times 306$; $P4_12_12$	~ 20
T70S(complex)[2] [b]	MPD	$524 \times 524 \times 306$; $P4_12_12$	12
T30S[3]	MPD	$407 \times 407 \times 169$; $P42_12$	7.3
H50S[4] [d]	PEG [a]	$212 \times 302 \times 567$; $C222_1$	2.9
T50S[5]	AS [a]	$495 \times 495 \times 196$; $P4_12_12$	8.7
B50S[6] [c,d]	PEG	$299 \times 547 \times 377$; 114°; C2	11

[a] MPD, PEG, AS = crystals are grown by vapor diffusion in hanging drops from solutions containing methyl-pentane-diol, polyethyleneglycol or ammonium sulphate, respectively.
[b] A complex of 70S ribosomes, 2 molecules phe-tRNA^{phe} and an oligomer of 35 uridines (as mRNA).
[c] Same for crystals of mutated 50S (lacking protein BL11) and of 50S bound to undecagold cluster.
[d] Small crystals of the same form of a complex of 50S + tRNA + a segment (18–20 mers) of a nascent protein chain[7].

tially the sedimentation behavior or the functional activity); the rational behind designing the ribosomal complexes which mimic functional states, including the choice of the mRNA. Furthermore, it was found that even when the exact values of the parameters are strictly kept, the conditions under which the best crystals grow may still vary in repeating experiments in an uncontrolled fashion. Therefore the subsequent low reproducibility in obtaining isomorphous crystals is not surprising. To minimize its level, the exact conditions for crystal growth are being screened for each preparation before the production of quality crystals.

The above list starts with the ribosomal source. Although it was known that under stressful conditions eukaryotic ribosomes tend to organize spontaneously in semi crystalline arrays, we chose to focus on prokaryotic ribosomes. These are relatively small, can be produced in high purity and large quantities and provide systems for in vitro crystallization which is independent of in vivo events, environmental influences and physiological factors which might be difficult or impossible to control and to reproduce. Among them, the halophilic ribosomes present an attractive system for investigating protein–RNA interactions since they function at salt concentrations which usually cause dissociation of nucleoprotein assemblages. It is noteworthy that despite these properties, the halophilic r-proteins and rRNA chains show reasonable homology to those of eubacteria as well as from eukaryotes [11]. The choice of ribosomes of halophilic and thermophilic bacteria resulted in major accomplishments that could have not been foreseen earlier. Perhaps the most striking and unexpected achievement is the growth of crystals of 50S ribosomal subunits from *Haloarcula marismortui*, which diffract well to almost atomic resolution, 2.9 Å, due to the addition of minute amounts of Cd^{2+} ion to the crystallization mixture containing above 2.5M of other ions.

All ribosomal crystals grown by us are extremely sensitive to X-rays. Their higher resolution terms decay within the first few seconds of irradiation. To minimize the radiation damage we pioneered data collection at cryo-temperature from shock frozen crystals. The diffracting power of the ribosomal crystals is so weak, that all stages of crystal analysis, including the characterization of the crystallographic parameters, must be carried out with bright synchrotron radiation, and require rather long exposures [12]. Interestingly, the determination of the accurate cell dimensions benefitted from the unusual length of the time required for data collection. For removing the uncertainties associated with inherent lack of isomorphism, the deviations in the wavelength and the fluctuations in beam direction, which are not negligible at large crystal-to-detector distances, advantage is being taken of the formation of microcrystals of ice on the outer surface of the spatula holding the irradiated frozen crystals. These accumulate during the long data-collection experiments and produce powder diffraction which can be accurately measured and serve for calibrating the above mentioned parameters and for determining the unit cell dimensions.

As a result of continuous refinements of the crystal growth conditions and the data collection protocols, the ribosomal crystallographic data are of reasonable quality, which in many cases is comparable to that obtained from crystalline proteins of average size [12] and may be used for phase determination [13]. A multi directional algorithm has been designed, exploiting the commonly used isomorphous replacement phasing method, side by side with efforts at very low resolution phasing by computational and semi experimental procedures. In this manuscript we highlight part of our phasing efforts, focusing on the interplay between the different approaches. Subsequent studies, aiming at the construction and the interpretation of higher resolution electron density maps are also being discussed.

2. Low resolution initial phasing by non-MIR methods

In small-molecule crystallography phases are routinely obtained by direct ab-initio methods. The relative ease and convenience of phasing by these methods stimulated considerable effort for their extension to macromolecules especially for cases, such as ribosomes, for which serious complications are expected in employing isomorphous replacement procedures.

2.1. Computational methods

Entropy maximization with log-likelihood gain as a phase-set discriminator [14,15] was used for phasing a data set of T50S at 89–250 Å resolution [16]. The main feature observed in the ME map resembles the shape of the reconstructed image of this particle [17] and the crystal packing motif displays a reasonable crystallographic net. These were further supported by the results of direct methods combined with ellipsoidal modelling [18], by the ultra low resolution R-factor searches at various solvent contrasts [13,16], by the few-atom-method (FAM [19]) calculations, and by low-resolution molecular-replacement studies [20], using the approximate model reconstructed for this particle [17].

An advanced approach, combining elements of direct methods, envelope refinement, maximum entropy filtering, likelihood ranking, cross-validation and cluster analysis, suitable for phasing at resolution up to 30 Å, was developed [21]. The results obtained by this method accord with the above mentioned attempts. In addition, applying it to data collected from native and derivatized H50S crystals provided tools for the localization of the heavy atom sites by difference Fourier calculations.

The use of reconstructed images of ribosomal particles of one bacterium with crystallographic data obtained from the same particle from other sources is based on the assumption that at the resolution limits of the reconstructions (28 Å) the gross structural features of prokaryotic ribosomes are rather similar. Thus, in addition to the studies described above, the image of B50S, reconstructed from the diffraction of a tilt series of negatively stained crystalline arrays [17] has been exploited for molecular replacement preliminary phasing of the H50S data [22,23].

2.2. Direct observation of crystal packing by electron microscopy

Since the large size of the ribosome enables its observation by electron microscopy, direct information about the packing motifs of ribosomal crystals has been obtained. In these experiments three-dimensional crystals are being embedded in epon and sectioned at preferred orientations to extremely thin slices, of a thickness similar to one unit cell. Visual inspection and symmetry considerations, sometime aided by optical diffraction, yielded valuable information about the packing arrangements in the crystals. In the case of B50S, the examination of the electron micrographs of the sections was combined with the results of real and reciprocal space searches and led to suggestions for a non-crystallographic three-fold symmetry, to the verification of the packing arrangements obtained by non-MIR methods at low resolution and to the determination of the number of the ribosomal particles in the asymmetric unit [24]. Similarily, the sections of T30S have been

Table 2
Typical results of solvent contrast experiments for T50S

Parameter	Native	2.0M $(NH_4)_2SeO_4$	0.5M GTG	1.0M GTG
Solvent-density	0.38 $e^-/Å^3$	0.41 $e^-/Å^3$	0.41 $e^-/Å^3$	0.44 $e^-/Å^3$
Cell-dimensions	502.0 Å, 197.0 Å	504.4 Å, 198.2 Å	500.0 Å, 195.0 Å	498.0 Å, 195.0 Å
a/c	2.523	2.545	2.564	2.538
Resolution-range	223–13 Å	250–13 Å	158–22 Å	248–21 Å
Potential resolution	8.5 Å	11.0 Å	14 Å	14 Å
Collected at	F1, CHESS, 1991	F1, CHESS, 1992	F1, CHESS, 1992	F1, CHESS, 1992
Wavelength	0.92 Å	0.91 Å	0.91 Å	0.91 Å
R_{merge} [a] ($I > 2\sigma(I)$)	6.56% (for 9459)	11.64% (for 3024)	–	–
R_{merge} [b] ($I > 2\sigma(I)$)	5.41% (for 1516)	6.84% (for 763)	7.19% (for 1795)	9.25% (for 3154)
R_{merge} [b] F^+ vs F^- (LR)	5.59% (for 628)	6.69% (for 331)	8.68% (for 550)	11.25% (for 590)
R_{merge} [b] Native vs ...	–	8.70% (for 540)	53.00% (for 768)	52.22% (for 798)
... Se–Soak vs ...	–	–	53.08% (for 468)	51.90% (for 598)
... 0.5M GTG vs ...	–	–	–	52.39% (for 998)

[a] 10–90 Å; [b] 30–300 Å.

exploited for reconfirming the packing motif computed by ab-initio methods [13].

2.3. Solvent contrast variation

Solvent contrast variation [25] is based on the active use of the contribution of the solvent to the structure factors in order to extract low resolution structural information. For this aim, the electron density of the solvent within the unit cell is being varied. Crystals of T30S, T50S and of the complex of T70S with 35(U) and 2 molecules of phetRNA^{phe} were immersed in solutions containing high amounts (0.3–1.5M) of goldthioglucose (GTG), a soluble compound of a very high electron density. Data were collected to the resolution limits mostly influenced by the solvent (> 12 Å). After the computational removal of contribution of the solvent, the resulting structure factors collected from T50S crystals were phased either by ME or by direct methods. The envelope which was elucidated in this way showed some similarity to the reconstructed image of B50S [17]. Some experimental results are reported in Table 2. Noteworthy is the pronounced anomalous effect, which encouraged the initiation of multi-wavelength anomalous solvent contrast (MASC) studies. As GTG is not soluble in the storage solution of H50S, which contains > 3.5M of ions, for performing SC measurements, the main constituent of the solution, KCl, is gradually being exchanged by compounds of a similar chemical nature, albeit heavier or lighter, such as CsBr, RbCl and LiCl.

3. Initial steps in phasing by isomorphous replacement

Because of the large size of the ribosome, ideal compounds for its derivatization are compact and dense materials of a large number of electrons. Multi-metal salts, such as polyheteroanions or coordination compounds (Table 3) are therefore used for derivatization by soaking, and dense metal clusters, such as undecagold [26] are covalently bound at specific sites prior to the crystallization. Simulation studies demonstrated the adequate phasing power of these compounds [24].

Table 3
Heavy atom compounds used for soaking

W18 = $(NH_4)_6(P_2W_{18}O_{62})14H_2O$
W30 = $K_{14}NaP_5W_{30}O_{110}$
W12 = $(K_5O_2)_3(PW_{12}O_{40})$
W17Co = $Cs_7(P_2W_{17}O_{61}Co(NC_5H_5))nH_2O$
$Na_{16}((O_3PCH_2PO_3)_4W_{12}O_{36})nH_2O$
$K_5H_4((phSn)_3(P_2W_{15}O_{59}))nH_2O$ (ph = phenyl)
$K_5H_4((buSn)_3(P_2W_{15}O_{59}))nH_2O$ (bu = butyl)
$K_7((buSn)_3(P_2W_{17}O_{61}))nH_2O$
$K_{11}H((buSnOH)_3(PW_9O_{34}))nH_2O$
$K_4H_3((buSn)_3(alfaSiW_9O_{31})_2)nH_2O$
$Cs_9H_6((buSnO)_3(alfaSiW_9O_{31})_2)nH_2O$
$Ta_6Br_{12}Cl_2 \cdot 8H_2O$[30]
$Ta_6Br_{14} \cdot 8H_2O$

3.1. Soaking experiments

Despite previous doubts, conditions for the derivatization of ribosomal crystals by soaking in solutions containing heavy atom compounds were found, and in several cases the data measured from soaked crystals proved to be suitable for low and medium resolution phasing. Specific examples are given below.

3.1.1. H50S: preliminary phasing at 7–9 Å resolution

These crystals grow as extremely thin plates, with typical size of $0.3 \times 0.3 \times 0.01$ mm^3, average cell dimensions of 212, 302 and 567 Å and symmetry: $C222_1$. Their resolution limits extend beyond 2.9 Å [4]. Partial phase information was obtained by soaking these crystals in solutions containing about 0.5mM of W30, W18, W12 and W17Co (Table 3 [27–30]). The resolution limits of the soaked crystals were found to be somewhat lower than those of the native ones. Most of the derivatives diffracted to 4–7 Å, and in many cases well shaped reflections were detected at 3.5 Å. However, because these compounds are expected to phase only to 6–7 Å, and due to technical reasons and synchrotron beam-time limitations, data were collected only to lower resolution.

The initial difference Patterson map was constructed at 12–40 Å resolution, using the data collected from a crystal soaked in W30. Initially individual W atoms were partially assigned. Within the

course of their refinement these converged to a few sites of the W30 cluster. These sites were confirmed by parallel efforts in which the W30 compound was treated as a group scatter as well as by ab-initio calculations using delta-F data. These 12 Å phases were used for constructing a SIR electron density map, which was subsequently subjected to two cycles of automatic solvent flattening [31], assuming that the crystals contain 65% solvent. The connectivity of the map was significantly enhanced when the reflections with resolution lower than 40 Å were included, and it contains features similar in size to those of the 50S subunit.

The 7–9 Å difference Patterson maps of the W12, W18 and W17Co derivatives contain non-interpretable Harker peaks. However, difference Fourier maps constructed for each of these derivatives using the phases derived for the W30 at 15 Å, revealed the positions of these clusters in the unit cell. After reconfirming these locations by careful examinations of the original non-interpretable difference Patterson maps, each of the sites was refined individually. Unfortunately, it was found that all four clusters occupy similar sites, therefore the phase information obtained from them could be used only for extending the resolution of the initial 12 Å resolution SIR map to 7–9 Å. The parameters of the phasing procedure are shown in Table 3 and the map in Fig. 1.

3.1.2. T30S: preliminary phasing at 19 Å resolution

T30S crystals grow as thin prisms of $0.3 \times 0.1 \times 0.05$ mm^3, with unit cell dimensions $a = b = 407$ Å and $c = 169$ Å and space group $P42_12$ or $P4_12_12$. Their highest resolution extends to 7.3 Å [3]. Soaking these crystals in solutions containing mM amounts of either W18 or W12 led to the extraction of preliminary phases. Because of uncertainties stemming from the extremely low intensities of the higher resolution reflections, the space-group of this crystal form was tentatively assigned to be $P42_12$, although absences supporting a 4_1 screw axis were observed. Efforts are currently being made at the determination of the right symmetry from the Harker peaks as well as from thin sections of embedded crystals, viewed by electron microscopy. The results shown in Fig. 2 and Table 4 were obtained for space group $P42_12$.

In the first stage a 30 Å SIR map was constructed for each derivative. The clusters were treated as group scatterers and no attempt was made to resolve the individual W atoms. The W12 cluster was approximated by a sphere, whereas the ellipsoid W18 cluster was represented by two adjacent scatterers,

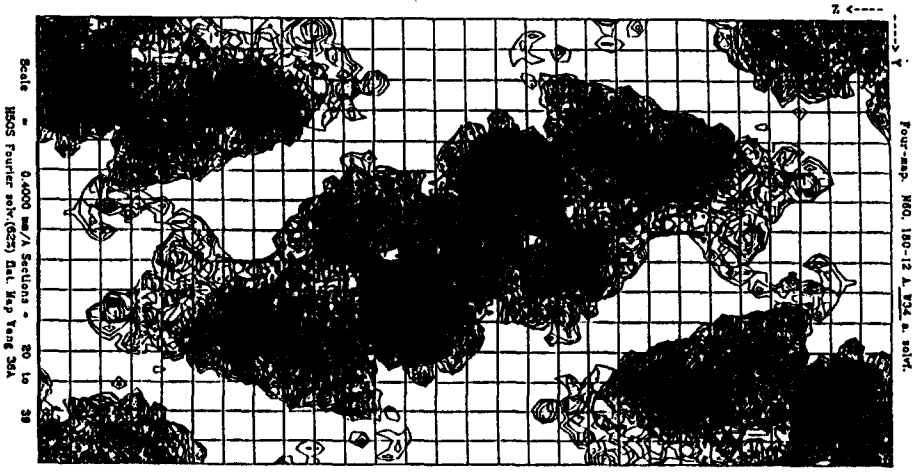

Fig. 1. The current electron density map of H50S. The MIR map at 9 Å resolution after several cycles of solvent flattening assuming 60% solvent. A projection of half a unit cell down the *a* axis is shown. The crystals were soaked for up to 34 days in solutions containing 1–2mM of the following clusters: $K_{14}NaP_5W_{30}O_{110}$, $(NH_4)_6(P_2W_{18}O_{62})14H_2O$, $(K_5O_2)_3(PW_{12}O_{40})$ and $Cs_7(P_2W_{17}O_{61}Co(NC_5H_5))nH_2O$. For all sets the Rmerge(I) = 8.4%–10.3% and the completeness is 74%–91%. Two major sites were located for the first two derivatives, 1 for the third and 4 for the fourth, with occupancies between 0.2 and 0.6. Phasing power between 0.7 (for the $W_{17}Co$ cluster) and 1.36 (for the W_{30} cluster). The overall figure of merit, after two cycles of solvent flattening (assuming 65% solvent) is 0.65.

each composed of nine W atoms. Combining the phase information from both derivatives yielded an un-interpretable 18–19 Å MIR electron density map. This was subjected to several cycles of automatic solvent flattening combined with density modification [31] assuming 66% of the crystal volume to be solvent. The main feature of this map (Fig. 2) may be interpreted as the small ribosomal particles, as it is similar to the representation obtained by subtracting the reconstructed image of the large ribosomal subunit from that of the whole ribosome [8,22,32]. The packing motif of the resulting electron density map (Fig. 2) is in accord with that seen in thin sections of embedded crystals and shows striking agreement with a map constructed from independent phase set obtained by ME combined with likelihood ranking [16].

3.2. Derivatization by covalent binding of heavy atom clusters: preliminary phasing by an undecagold cluster

A SIR electron density map of B50S was obtained at 26 Å resolution using a heavy atom derivative formed by specific quantitative derivatization with a dense undecagold cluster [24]. Crystals of B50S are grown as monoclinic prisms with maximum dimensions of $0.8 \times 0.2 \times 0.04$ mm^3. Their space group is C2, with unit cell dimensions of a = 300, b = 547, c = 377 Å and beta = 111.9° (Table 5). Among the

Table 4
The parameters of the soaking experiments

	Native	Wo(30)	Wo(18)	K-Wo(12)	Co-Wo(17)
(a) H50S					
Unit cell (Å)			212 302 567 90 90 90		
Space group			$C222_1$		
Resolution (used)	5.2 Å	12 Å	7.0 Å	9.0 Å	9.0 Å
R_{merge}	0.084	0.101	0.124	0.095	0.103
Completeness	74.4%	78%	91%	70%	78%
R_{deriv}		0.25	0.15	0.30	0.19
No. of major sites [a]		2(4)	2(4)	1(2)	4(5)
R_{cullis} [b]		0.80(0.70)	0.89(0.89)	0.75(0.88)	0.90(0.90)
Phasing power [b]		1.36(0.88)	0.8(0.52)	1.39(0.9)	0.70(0.43)

	Native	Wo(12)	Wo(18)	Ta_6Br_{14}
(b) T30S				
Unit cell (Å)			407 407 169 90 90 90	
Space group			$P42_12$	
Resolution	290–15 Å	83–12 Å	50–15 Å	98–10 Å
R_{merge}	0.077	0.075	0.087	0.078
Completeness	64%	60%	60%	74%
R_{deriv}		0.35	2	–
No. of major sites [a]		3(5)	2	–
R_{cullis} [b]		0.83(0.76)	0.76(0.65)	–
Phasing power [b]		1.61(1.22)	1.9(1.78)	–

[a] Numbers in parenthesis are possible extra sites.
[b] Numbers in parenthesis are for centric reflections.

$$R_{merge} = R_{sym} = \sum_h \sum_i |I_{hi} - I_h| / \sum_h |I_h|,$$

where h denotes reflection hkl and n is its symmetry related one.

$$R_{deriv} = \sum_n |I^n_{nat} - kI^n_{deriv}| / \sum_n |I^n_{nat}|,$$

where nat denotes the reflections collected from the native crystals and deriv from the derivatized one.

ribosomal crystals, these are the most unstable and require the longest measuring time because of their low symmetry and their extremely weak diffraction power. They suffer from significant non-uniform mosaicity, of 0.3°–1.0° and in several cases the variations in cell constants were over 1%, indicating lack of isomorphism. Despite these shortcomings, these crystals were chosen for testing the phasing potential of covalently bound clusters, because (1) B50S particles possess only one exposed –SH on a protein (BL11) which can be reversibly detached from the ribosome, and (2) it was shown that this –SH is suitable for binding large chemical entities in a fashion which does not hamper its incorporation into core particles lacking these protein, prepared by the addition of the antibiotic thiostrepton to the bacterial growth medium. The mere bacterial growth without protein BL11, alongside with the crystallization of the cores lacking this protein under the same conditions as used for the native particles, indicate that the removal of BL11 does not cause gross conformational changes in the ribosome, and that the contribution of this protein to the crystal network is not crucial.

For quantitative binding the undecagold cluster was prepared as a monofunctional reagent, specific to free sulfhydryls, by attaching to it a short aliphatic chain with a maleimido or an iodoacetyl group at its

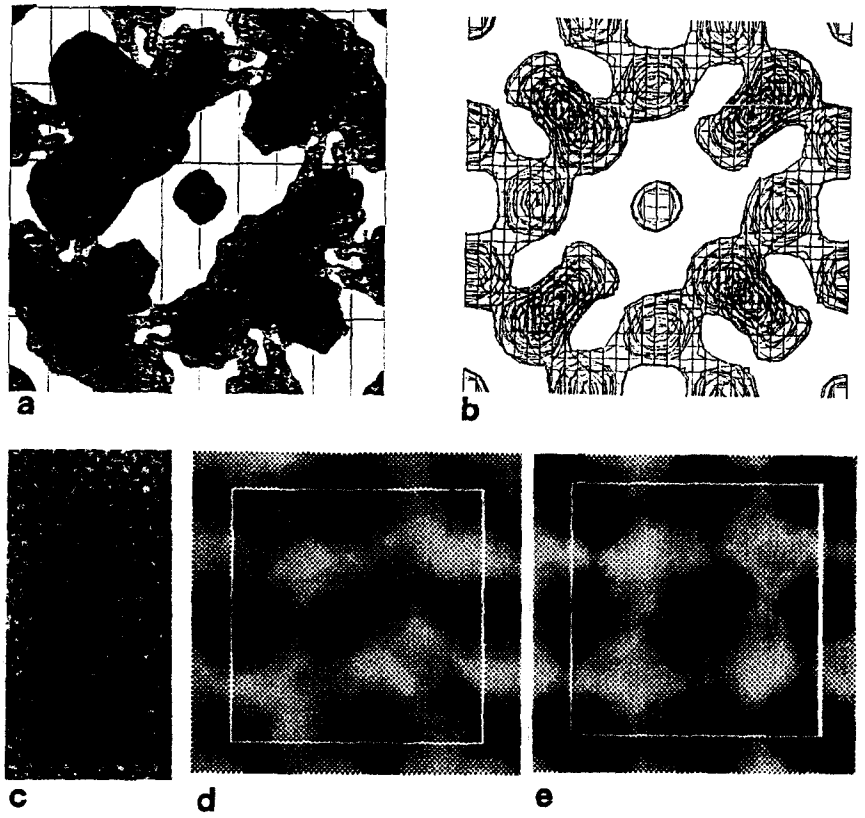

Fig. 2. The current preliminary electron density maps of T30S. (a) The MIR map at 19 Å resolution after several cycles of solvent flattening assuming 66% solvent, with final figures of merit of 0.59 and 0.38 for the centric and acentric reflections, respectively. The whole unit cell is shown, down the c axis. The crystals were soaked for 43 and 14 h in solutions of 3mM of $(NH_4)_6(P_2W_{18}O_{62})14H_2O$ and $(K_5O_2)_3(PW_{12}O_{40})$, respectively. Two major sites were located for the first derivative, and five for the second. The latters were partially located in the difference Patterson map and partially in difference Fourier, exploiting the phase information obtained by the first derivative. The combined MIR figure of merit is 0.67. (b) The 40–50 Å map constructed with ab initio phases. (c) A positively stained thin section of embedded T30S crystal. (d) Comparison between the observed filtered image of (c) and (e) the simulated packing arrangement, based on the ab initio phases.

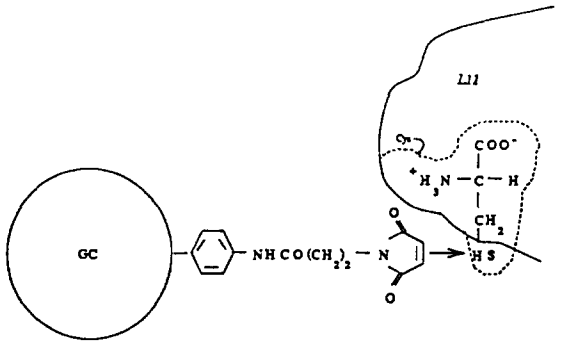

Fig. 3. The monofunctional reagent of the undecagold cluster used for the derivatization and the mode of its binding.

Fig. 4. Left: Projection of the whole unit cell, down the z direction, after two cycles of solvent flattening and phase combination of the 26 Å electron density map of B50S. Right: A section of 50 Å thickness of the map shown on the left.

end. The latter was designed to avoid the potential chirality of the maleimido moiety. The monofunctional reagent of the undecagold cluster was bound to isolated protein BL11 by reacting with its only cysteine (Fig. 3). Although the binding of the cluster was carried out under denaturing conditions, and although the molecular weight of the undecagold cluster (6.2 kDa) approaches half of that of BL11 (15.5 kDa) and its overall size (22 Å in diameter) approaches the dimensions of a typical r-protein, the gold-cluster bound protein reconstituted into cores of mutated ribosomes lacking BL11, yielding fully derivatized particles [9,24,33].

The undecagold cluster contains a core of 8.2 Å diameter, consisting of eleven gold atoms linked directly to each other, surrounded by hydrophilic organic groups forming a unique, well-defined compound [26]. The usable crystallographic data measured from some of the B50S crystals extend to 15 Å, although their diffraction pattern contains reflections at 11 Å. However, it was found that for obtaining consistent results, the resolution had to be further limited, to 20 Å. Due to the pronounced lack of isomorphism of these crystals, four data sets of native, four of the derivative and one of the mutated crystals had to be collected until a sufficiently isomorphous couple was detected. It was found that for this combination, the phasing power of the undecagold cluster increases with the resolution (average value = 1.2) within the 26–50 Å shell. The R_{Cullis} for the first SIR phase calculation was 0.64

Table 5
The quality of the B50S data

	Data set#	R_{max} (Å)	R_{min} (Å)	Unique ref	R_{merge} %	Cell dimensions [a] (Å)				$D(v)$ (%)
						a	b	c	β (deg)	
NAT	21	14.9	91.3	5561	6.9	297.6	547	383.3	111.6	+1.068
	16	14.4	88.5	5226	7.8	302.9	547	374.4	112.2	+0.057
	19	18.0	176.0	4891	7.2	300.0	547	377.0	111.9	0.000
	46	21.0	93.0	2945	7.3	297.3	547	376.0	111.1	+0.618
DER	48	14.0	97.0	4535	14.2	302.9	547	374.4	112.2	+0.057
	41	12.8	124.7	8331	7.4	300.0	547	377.0	111.9	+0.000
	53	15.7	62.2	4808	9.5	300.0	547	377.0	111.9	0.000
	39	22.0	245.0	1416	7.4	300.0	547	382.0	111.9	+1.326
M	83	16.0	49.0	5104	10.4	293.1	547	372.8	111.4	−3.053

NAT = native; DER = derivative, M = mutant.
[a] The cell axes were scaled to a common b axis (d_{010} = 547 Å).
$D(v)$ = the change in crystal volume (compared to crystal #41).

with a figure of merit of 0.42. To assist in resolving the phase ambiguity and to improve the quality of the Fourier map, solvent flattening [31] assuming 61% solvent, followed by phase combination was applied. Convergence was reached after two cycles. The figure of merit was increased to 0.71 with an R-factor of 0.44.

The resulting electron density map (Fig. 4) has density regions consistent in size to three 50S subunits in the asymmetric unit, in accord with the non-crystallographic symmetry revealed by self rotation searches as well as in electron micrographs of sectioned crystals. However, so far it has not been possible to fully distinguish between the individual particles.

3.3. Problems encountered during the course of phasing

The studies described above established that phase information can be obtained from ribosomal crystals by derivatization with heavy metal clusters, even when the crystals under investigation are unstable and weakly diffracting. However, several obstacles hampering smooth data collection and phasing have been encountered, connected with rather sophisticated as well as more trivial aspects. Examples are the negative correlation between the life time of irradiated shock frozen crystals and the brightness of the synchrotron beam; the need to reduce the size of the clusters to enable higher resolution phasing, which in turn, necessitates quantitative binding of small clusters at multiple sites; the difficulties resulting from the non-uniform mosaic spread, which at extremes lead to the production of multiple diffraction patterns while measuring one crystal; and the limitations imposed by the physical constants of the SR stations, the properties of the detectors and the allocation of measuring time.

By far, the most serious problem in phasing the ribosomal crystallographic data stems from the low level of the isomorphism of the ribosomal crystals. Thus, deviations from isomorphism have been observed even between crystals grown under the same conditions from the same ribosomal preparation in the same drop. As mentioned above, because of the significant lack of isomorphism of the B50S crystals a thorough search for an isomorphous couple had to be conducted in order to produce a reliable difference Patterson map [24]. To minimize the tediousness and inefficiency associated with such studies (carried out in this way mainly due to our initial ignorance of the severeness of the problem of non-isomorphism), we have attempted using cut crystals. Independent determination of the cell dimensions of each part of segmented crystals indicated the high reproducibility of the shock cooling process, and showed that the fragments produced from one crystal do not show deviations from isomorphism [34]. At present we face sever problems concerning our cutting procedures, as most of the ribosomal crystals are too soft to resist the mechanical stresses associated with the fragmentation. Once a procedure for smooth and non-damaging cutting is designed, pairs (or larger number) of data sets can be collected from the same crystal. Thus, native data will be collected from one part of a cut crystals and the other part(s) will be measured after being soaked and derivatized.

An alternative approach to overcome the low level of isomorphism is the exploitation of the MAD phasing procedure. In contrast to MIR which requires collecting data from native and heavy atom derivative crystals, for MAD one crystal should be sufficient, providing that there is no radiation decay while measuring a few data sets, each at a different wavelength. Some comments about the application of this method to our systems are given below.

4. Specific labeling for higher resolution phasing

4.1. Multi-site binding of heavy atom clusters

The demonstrated feasibility of covalently bound clusters for low resolution phasing encouraged investing further effort at specific derivatization of the ribosomal crystals which diffract to higher resolution (H50S and T30S). Anticipating higher resolution maps, heavy atoms bound at pre-determined sites are expected to contribute significantly not only in phasing, but also in the localization of the sites to which the heavy atoms are bound, a valuable information for the course of map interpretation. To reach phasing at higher resolution, smaller compounds, such as a tetrairidium cluster [35] or TAMM are being exploited. In addition, the synthesis of compact clusters

of W or a similar metal, designed for specific binding, is underway (M. Pope, personal communication). As single clusters may not possess sufficient electron density, for obtaining measurable effects, procedures are being developed for their multi-sites covalent binding at pre-determined locations. As seen below, these efforts require considerable biochemical and genetic efforts.

4.2. The prospects for MAD phasing

The rather low degree of isomorphism of the ribosomal crystals directed our attention to phasing by MAD. Derivatization for MAD is essentially the same as performed for MIR. However, until recently, MAD has been used to a lesser extent because the experimental requirements for data collection are much more demanding. Thus, the anomalous signal is roughly 10 times lower than that obtained per heavy atom with MIR. As in MIR experiments, for enhancing the probability of obtaining measurable anomalous signals at higher resolution, multi-site binding of dense and compact small clusters is required. Within this frame, procedures are being developed for the fascinating prospect of enhancing the phasing power by performing multi-MAD experiments, namely, simultaneous derivatization with more than one powerful heavy atom scatterer. In soaking experiments, Ta_6Br_{14} [36,37] is an attractive compound, as it contains two different moieties (Ta and Br) with a significant anomalous signal. For the cases of multi-site covalent derivatization, the genetic engineering of several different binding sites, required for enhancing the phasing power, facilitates the covalent binding of different scatterers at predetermined locations.

4.3. The extension of the binding protocols to the halophilic and thermophilic systems

It was found that it was not possible to apply a straight forward extension of the procedures developed for binding the gold cluster to B50S or H50S and T30S, as there are no naturally exposed sulfhydrils on their surfaces suitable for derivatization. Thus, in contrast to the relative ease of the incorporation of the gold-cluster-bound BL11 into cores lacking it, protein HmaL11, the halophilic homolog of BL11 [9,38], can be reconstituted into core H50S particles only when its sulfhydryl group is free. In addition, because of the significant resistance of the halophilic ribosomes to mutagenesis, no protein-depleted core particles could be produced by growing the bacteria on medium containing antibiotics. Also, the experimental conditions under which quantitative detachment of selected *E. coli* r-proteins occurs, were found unsuitable for the halophilic and the thermophilic systems.

Consequently, potential heavy-atom binding sites are being either created by chemical modifications, or inserted by genetic procedures [10,38,39]. For choosing appropriate locations for these insertions, special procedures for specific quantitative detachment and reconstitution of selected ribosomal proteins have been developed, and the surfaces of these ribosomal particles are being mapped by chemical and enzymatical methods. For the surface mapping experiments as well as for the insertion of the binding sites, sequence information is essential. So far over a third of the ribosomal proteins from *T. thermophilus* [40], and more than two thirds of those from *H. marismortui* have been fully or partially sequenced [10].

4.4. Surface characterization

An exact definition of the surface of the halophilic and the thermophilic ribosomes is currently not possible, as the parameters influencing the ribosomal compactness have not yet been fully identified. Nevertheless, several experiments focusing on the exposed regions of the rRNA as well as of the r-proteins are being carried out.

4.4.1. Probing exposed single stranded rRNA by complementary DNA oligomers

Probing exposed single stranded rRNA by complementary DNA oligomers gained recently considerable popularity. As the exposed rRNA regions which are involved in functional activity are rather conserved, several such regions could be located on halophilic and thermophilic ribosomes by analogy to *E. coli*. DNA oligomers, targeting these rRNA regions, have been synthesized. These may also be used for specific derivatization, as they can be prepared with a thiol group at their 5′ or 3′ ends.

Among the various undecabase oligomers, the tightest hybridization was obtained for the sequence 5′-AAGGAGGTGAT-3′, complementing the "anti-Shine-Dalgarno" region of the 16S rRNA in T30S. Sucrose gradient centrifugation was performed to purify the hybrid from the unbound oligomers, and the hybridized particles with the natural as well as the thiol modified oligonucleotide were crystallized [10]. In parallel experiments, exposed stretches of the 23S rRNA of H50S including bases 1422–1432, the so called "thiostrepton binding site" and bases 2646–2667, the "alfa-sarcin binding site" have been hybridized [39].

4.4.2. Chemical probing of exposed ribosomal proteins

Earlier accessibility studies were concentrated on limited proteolysis under conditions optimized for *E. coli*. Attempts to extend the proteolytic experiments to the halophilic ribosomes were only partially successful, because the halophilic ribosomes require high salinity for maintaining their compactness, whereas the conditions suitable for the proteolytic reaction of all the commercially available enzymes are milder. Therefore, even when using robust proteolytic mixtures, partial unfolding of the halophilic ribosomes could have occurred. Such unfolding may not effect dramatically the overall sedimentation coefficient, showing that the gross integrity of the ribosomes has not been altered, but at the same time, an opening-up of the compact active conformation and the consequent exposure of internal residues cannot be ruled out. An alternative procedure is to decorate the surface of the ribosomes by chemical means. Two exposed moieties are being probed: cysteines and free amines [10,33,39,41]. The probed proteins were detached from the particle, digested with the endoproteinse Lys-C from isobacter enzymogene, and the resulting peptides were analyzed for labeled lysines in their peptide maps.

4.5. Site directed mutagenesis

The surface mapping experiments were synchronized with the identification of the genes coding for the detachable proteins. These proteins were overproduced in *E. coli*, using the pET expression system [42]. Despite the relatively low intracellular salt concentration of *E. coli*, the halophilic overexpressed proteins reached the level of 30–40% of the total cell proteins and remained soluble in the cytoplasm. Unexpected complications were encountered in attempts at cloning HmaL12 and the HmaL12/HmaL10 gene complex into the overexpression vectors, presumably because of unusual stable folding of this gene region. These were overcome by the design of the appropriate oligonucleotide primers according to the thermodynamic algorithm [10].

Site directed mutagenesis for insertion of cysteines on the r-proteins which can be reversibly detached from H50S is currently in progress. To avoid undesired binding of the heavy atom cluster, we first exchanged the cysteine of HmaL11, which, as mentioned above, once probed by –SH reagents, was found to prevent the incorporation of the protein into core particles [9]. The production of core particles, depleted of protein HmaL11, simplifies the analysis of the incorporation of the mutated protein HmaL11. With the exception of two mutants, all could be incorporated into the depleted core particles. The differences in the ability to incorporate may indicate in-situ interactions or suggest that the genetic manipulations led to conformational changes which can not be tolerated by the ribosomal cores.

5. The isolation and characterization of in-situ complexes

The knowledge of the accurate structures of ribosomal components should provide a powerful tool for higher resolution structure determination of the entire particle. We anticipate to benefit from the crystallographic analysis of the structures of isolated r-proteins, performed elsewhere [43,44], although it remains to be seen whether their structures in isolation reflect their in-situ conformations. Internal small sub-structures are more likely to maintain their native conformation, as they may keep their in-situ micro environment. During the course of the surface mapping and depletion studies on H50S, two in situ stable complexes have been identified. One is a ribonucleic protein containing HmaL1 and a stretch of about 120 nucleotides of 23S rRNA [11]. Interestingly, despite the "exotic" properties of the

halophilic ribosomes and the evolutionary distance between the halophiles and *E. coli*, it was found that both archaebacterial components of this complex are readily interchangeable with their eubacterial counterparts.

The existence of a complex between proteins HmaL10 and HmaL12 was revealed by the comparison of the two-dimensional gels of the total proteins of H50S and those belonging to the group of proteins which can be detached reversibly. Initial quantitative analysis showed that this complex contains four copies of protein HmaL12 and one of HmaL10, similar to the composition found in eubacterial, eukaryotic and other archeabacterial ribosomes [45–47]. The halophilic complex is remarkably stable. It does not disintegrate at 8M urea or under the FPLC conditions and only dioxane and SDS caused its separation. Therefore it is expected to form ordered crystals of a higher quality than that obtained for its homolog from *B. stearothermophilus* [48].

As all components of the two complexes have been overexpressed, they are being produced in amounts sufficient for their crystallization as well as for their derivatization and incorporation into core particles. In addition, all three proteins participating in these complexes are members of the group of detached r-proteins, indicating that they are located at the particle's surface, thus providing potential cluster binding sites. The combination of the anticipated high resolution structures of these complexes with the knowledge of the cluster binding locations on them, should be valuable for the interpretation of the electron density map of the entire particle.

6. Crystals of complexes mimicking defined functional states

Images of the B70S ribosome and its large subunit reconstructed by us from the diffraction of electron micrographs of tilt series of crystalline arrays at 47 and 28 Å respectively, revealed several key features, not detected earlier, associated mainly with internal vacant or partially filled hollows [17,49]. Their provisional interpretation suggested that the biosynthetic reaction occurs at the intersubunit interface, that mRNA progresses along a groove in the small subunit and that the sheltered paths of the nascent proteins is a tunnel, within a system of tunnels, spanning the large subunit [17,22,32,50] and led to modelling results of biochemical experiments which suggest partial folding of nascent proteins within their exit tunnel in a feasible way [51,52]. Interestingly, at much higher resolution (15 Å) the internal main tunnel has been observed even in filtered images of two-dimensional sheets [53].

The sizable intersubunit void may be associated with the potential ribosomal flexibility, which may reduce the homogeneity within the ribosomal populations and consequently limit the quality of their crystals. As this void was assigned to host the non-ribosomal components participating in protein biosynthesis [32], it was expected that a rational design of complexes which are supposed to "fill" up the void will increase the homogeneity and introduce rigidity. Indeed, even the very simple complex, composed of 70S ribosome, two phetRNA^{phe} molecules and a chain of about 35 uridyl residues, led to a dramatic improvement in the reproducibility of crystal growth and to an increase of over 10 Å in the resolution limits [2].

More sophisticated complexes of T70S have been recently designed, aimed at increasing the homogeneity of the complexes and at minimizing the chances of protruding stretches of mRNA. These contain around 18 nucleotides, as this is the approximate length of mRNA on both sides of the decoding site, which is masked by the ribosome [56]. Best results were obtained for $(ATC)_5$-CTT. Including in the reaction mixture charged tRNA^{ile} and omitting tRNA^{leu}, crystals of the complex with an average of 1.6 molecules of ile-tRNA^{ile} per ribosome have been obtained.

As tRNA participates in all so far crystallized complexes of ribosomal particles trapped at defined functional states (the above mentioned complexes of T70S as well as those of 50S subunits with one tRNA molecule and a short segment of nascent polypeptide [7]), a procedure was designed for specific labeling tRNA^{phe} and tRNA^{leu} by multi-metal clusters, in a fashion which does not hamper the tRNA synthetase activity and the binding of the charged tRNA to the ribosome [41]. The complexes containing the gold-cluster bound tRNA molecules were crystallized and are being exposed to crystallographic analysis.

Recently, somewhat higher resolution reconstructions of E70S, performed on single particles embedded in vitreous ice, were reported to show essentially the same prominent features [54,55] which were previously detected by us [17,32,49]. Gratifying is the fact that in both studies the interpretations of the internal features are based on our original suggestion: the intersubunit free space is being utilized as the center of the peptidyl transferase activity and at least one of the tunnels in the large subunit is the path of the progressing nascent chains.

7. Conclusions and prospects

Our approach in pursuing the crystallographic studies of ribosomes is to exploit the extensive information available on the genetic, functional and chemical properties of ribosomes for a rational design of protocols for crystallization and for derivatization with dense clusters or multi-atom salts. Indeed, these efforts led to initial phasing and the construction of preliminary electron density maps at intermediate resolution which show features of the size expected for the corresponding ribosomal particles. Since the crystals of H50S and T30S diffract to 2.9 and 7.3 Å, respectively, and since the extension of the derivatization procedures to these particles is well underway, a higher resolution map is anticipated in the foreseeable future.

8. Abbreviations

70S 30S 50S: bacterial ribosomes and their small and large subunits, respectively (named according to their sedimentation coefficients).
E,B,T,H as a prefix indicate the bacterium (*Escherichia coli*, *Bacillus stearothermophilus*, *Thermus thermophilus*, *Haloarcula marismortui*, respectively).
rRNA: ribosomal RNA.
r-Proteins: ribosomal proteins.
For r-proteins: L stands for 50S, and S for 30S (e.g. BL11 is protein 11 from B50S).
HmaL# indicates that protein # from H50S is homologous to protein # from E50S.
cDNA: DNA oligomers, complementary to rRNA.
SR: synchrotron radiation.
MIR, SIR: multiple and single isomorphous replacement.
MAD: multiple wavelength dispersion.
ME: maximum entropy.
SC: solvent contrast.
SDS: sodium dodecyl sulfate.
FPLC: Fast Protein Liquid Chromatography.
TAMM: tetrakis (acetoxymercuri) methane.

Acknowledgements

We owe exceptional gratitude to the late Prof. H.G. Wittmann with whom we initiated these studies, and to the late Dr. K.von Böhlen who developed the experimental crystallographic aspects enthusiastically. We thank Drs. M. Pope and W. Jahn for their gifts of multi-metal compounds, M. Roth, E. Pebay-Peyroula, K.R. Leonard, W. Chiu, W. Hill, B. Hardesty, A. Horovitz, T. Choli and A. Podjarny, for their active participation in different aspects of our studies and for their illuminating comments, Drs. G. Bricogne, C. Gilmore and C. Carter for providing their programs and advice, Dr. F. Triana for preparing tRNA molecules and Drs. T. Leighton and J. Schnier for producing the mutant. We are also grateful to the excellent experimental assistance provides by Ms. C. Glotz, R. Albrecht, C. Paulke, J. Müssig, J. Piefke, R. Hasenbank, B. Romberg, I. Dunkel, B. Schroeter, S. Meyer, C. Radzwil, B. Donzelmann, M. Laschever and P. Baruch as well as Mr. K. Knaak and T. Arad.

Data were collected at the following synchrotron facilities: EMBL and MPG beam lines at DESY, Hamburg; CHESS, Cornell University; SSRL, Stanford University; and PF/KEK, Japan. Support was provided by the Max-Planck Society, the US National Institute of Health (NIH GM 34360), the German Ministry for Science and Technology (BMFT 05-641EAC) and the Kimmelman Center for Macromolecular Assembly at the Weizmann Institute. A.Y. holds the Martin S. Kimmel Professorial Chair.

References

[1] Z. Berkovitch-Yellin, H.A.S. Hansen, W.S.Bennett, R. Sharon, K. von Böhlen, N. Volkmann, J. Piefke, A. Yonath and H.G. Wittmann, J. Crystal Growth 110 (1991) 208.

[2] H.A.S. Hansen, N. Volkmann, J. Piefke, C. Glotz, S. Weinstein, I. Makowski, S. Meyer, H.G. Wittmann and A. Yonath, Biochem. Biophys. Acta 1 (1990) 1.
[3] A. Yonath, C. Glotz, H.S. Gewitz, K. S. Bartels, K. von Böhlen, I. Makowski and H.G. Wittmann, J. Mol. Biol. 203 (1988) 831.
[4] K. von Böhlen, I. Makowski, H.A.S. Hansen, H. Bartels, Z. Berkovitch-Yellin, A. Zaytzev-Bashan, S. Meyer, C. Paulke, F. Franceschi and A. Yonath, J. Mol. Biol. 222 (1991) 11.
[5] N. Volkmann, S. Hottentrager, H.A.S. Hansen, A. Zaytzev-Bashan, R. Sharon, Z. Berkovitch-Yellin, A. Yonath and H.G. Wittmann, J. Mol. Biol. 216 (1990) 239.
[6] J. Müssig, I. Makowski, K. von Böhlen, H. Hansen, K.S. Bartels, H.G. Wittmann and A. Yonath, J. Mol. Biol. 205 (1989) 619.
[7] H.S. Gewitz, C. Glotz, J. Piefke, A. Yonath and H.G. Wittmann, Biochimie 70 (1988) 645.
[8] Z. Berkovitch-Yellin, W.S. Bennett and A. Yonath, Crit. Rev. Biochem. Mol. Biol. 27 (1992) 403.
[9] F. Franceschi, S. Weinstein, U. Evers, E. Arndt, W. Jahn, H.A.S. Hansen, K. von Böhlen, Z. Berkovitch-Yellin, M. Eisenstein, I. Agmon, J. Thygesen, N. Volkmann, H. Bartels, F. Schlünzen, A. Zaytzev-Bashan, R. Sharon, I. Levin, A. Dribin, I. Sagi, T. Choli-Papadopoulou, P. Tsiboly, G. Kryger, W.S. Bennett and A. Yonath, in: The Translation Apparatus, Ed. K. Nierhaus (Plenum, New York, 1993) p. 397.
[10] F. Franceschi, S. Weinstein, I. Sagi, M. Peretz, V. Weinrich, S. Morlang, N. Böddeker, M. Geva, I. Levin, I. Agmon, Z. Berkovitch-Yellin, F. Schlünzen, H.A.S. Hansen, H. Bartels, W.S. Bennett, N. Volkmann, J. Thygesen, J. Harms, A. Zaytzev-Bashan, S. Krumbholz, R. Sharon, A. Dribin, E. Maltz and A. Yonath, in: Biological Structure and Dynamics, Eds. R.H. Sarma and M.H. Sarma (Adenin, 1996) pp. 25–41.
[11] U. Evers, F. Franceschi, N. Boeddeker and A. Yonath, Biophys. Chem. 50 (1994) 3.
[12] Z. Berkovitch-Yellin, H.A.S. Hansen, S. Weinstein, M. Eisenstein, K. von Böhlen, I. Agmon, U. Evers, J. Thygesen, N. Volkmann, H. Bartels, F. Schlünzen, A. Zaytzev-Bashan, R. Sharon, I. Levine, A. Dribin, G. Kryger, W.S. Bennett, F. Franceschi and A. Yonath, in: Synchrotron Radiation in Biosciences, Eds. B. Chance et al. (Clarendon, Oxford, 1994) p. 61.
[13] F. Schlünzen, H.A.S. Hansen, J. Thygesen, W.S. Bennett, N. Volkmann, I. Levin, J. Harms, H. Bartels, A. Zaytzev-Bashan, Z. Berkovitch-Yellin, I. Sagi, F. Franceschi, S. Krumbholz, M. Geva, S. Weinstein, I. Agmon, N. Böddeker, S. Morlang, R. Sharon, A. Dribin, E. Maltz, M. Peretz, V. Weinrich and A. Yonath, J. Biochem. Cell Biol. 73 (1995) 739.
[14] G. Bricogne, Acta Cryst. A 40 (1984) 410.
[15] G. Bricogne and C. J. Gilmore, Acta Cryst. A 46 (1990) 284.
[16] N. Volkmann, in: Entropy, Likelihood, Baysian Inference and their Application in Crystal Structure Determination, Ed. G. Bricogne (Am. Cryst. Assoc., 1995), in press.
[17] A. Yonath, K.R. Leonard and H.G. Wittmann, Science 236 (1987) 813.
[18] M. Roth and E. Pebay-Peyroula, in: Entropy, Likelihood, Baysian Inference and their Application in Crystal Structure Determination, Ed. G. Bricogne (Am. Cryst. Assoc., 1995), in press.
[19] V.Y. Lunin, N.M. Lunina, T.E. Petrova, E.A. Vernoslava, A.G. Urzhumstev and A.D. Podjarny, Acta Cryst. D 51 (1995) 896.
[20] A.G. Urzhumstev and A.D. Podjarny, Acta Cryst. D 51 (1995), in press.
[21] N. Volkmann, F. Schlünzen, E.A. Vernoslava, A.G. Urzhumstev, A.D. Podjarny, M. Roth, E. Pebay-Peyroula, Z. Berkovitch-Yellin, A. Zaytzev-Bashan and A. Yonath, Joint CCP4 and ESF-EACBM Newsletters (June 1995) 25.
[22] Z. Berkovitch-Yellin, H.G. Wittmann and A. Yonath, Acta Cryst. B 46 (1990) 637.
[23] M. Eisenstein, R. Sharon, Z. Berkovitch-Yellin, H.S. Gewitz, S. Weinstein, E. Pebay-Peyroula, M. Roth and A. Yonath, Biochemie 73 (1991) 897.
[24] H. Bartels, W.S. Bennett, H.A.S. Hansen, M. Eisenstein, S. Weinstein, J. Müssig, N. Volkmann, F. Schlünzen, I. Agmon, F. Franceschi and A. Yonath, J. Peptide Sci. 37 (1995) 411.
[25] C.W. Carter, Jr., K.V. Crumley, D.E. Coleman, F. Hage, Acta Cryst. A 46 (1990) 57.
[26] W. Jahn, Z. Naturforsch. 44b (1989) 1313.
[27] M.H. Alizadeh, S.P. Harmalker, Y. Jeannin, J. Martin-Frere and M.T. Pope, J. Am. Chem. Soc. 107 (1995) 2662.
[28] B. Dawson, Acta Cryst. 6 (1953) 113.
[29] G.M. Brown, M.R. Noe Spirlet, W.R. Busing and H.A. Levy, Acta Cryst. B 33 (1977) 1038.
[30] M.T. Pope, private communication.
[31] B.C. Wang, Methods Enzymol. 115 (1985) 90.
[32] A. Yonath and H.G. Wittmann, TIBS 14 (1989) 329.
[33] S. Weinstein, W. Jahn, H. Hansen, H.G. Wittmann and A. Yonath, J. Biol. Chem. 264 (1989) 19138.
[34] J. Harms, F. Schlünzen, K. von Böhlen, J. Thygesen, S. Meyer, I. Dunkel, B. Donzelmann, H.A.S. Hansen, A. Zaytzev-Bashan, A. Dribin, G. Kryger, G. Thoms, N. Volkmann, H. Bartels, W.S. Bennett and A. Yonath, ESF (May 1993) 26.
[35] W. Jahn, Z. Naturforsch. 44b (1989) 79.
[36] G. Schneider and Y. Lindqvist, Acta Cryst. D 50 (1994) 186.
[37] J. Löwe, D. Stock, B. Jap, P. Zwickl, W. Baumeister and R. Huber, Science 268 (1995) 533.
[38] F. Franceschi, I. Sagi, N. Böddeker, U. Evers, E. Arndt, C. Paulke, R. Hasenbank, M. Laschever, C. Glotz, J. Piefke, J. Müssig, S. Weinstein and A. Yonath, Syst. Appl. Microbiol. 16 (1994) 697.
[39] I. Sagi, V. Weinrich, I. Levin, C. Glotz, M. Laschever, M. Melamud, F. Franceschi, S. Weinstein and A. Yonath, Biophys. J. 55 (1995) 31.
[40] P. Tsiboli, E. Herfurth and T. Choli, Eur. J. Biochem. 226 (1994) 169.
[41] S. Weinstein, W. Jahn, M. Laschever, T. Arad, W. Tichelaar, M. Haider, C. Glotz, T. Boeckh, Z. Berkovitch-Yellin, F. Franceschi and A. Yonath, J. Crystal Growth 122 (1992) 286.
[42] F.W. Studier, A.H. Rosenberg, J.J. Dunn and J.W. Dubendorf, Methods Enzymol. 185 (1990) 60.
[43] A. Liljas, Curr. Opinion Struct. Biol. 5 (1995) 721.

[44] A. Yonath and F. Franceschi, Curr. Opinion Struct. Biol. 3 (1993) 45.
[45] W. Moller and J.A. Maasen, in: The Ribosome, Eds. B. Hardesty and G. Kramer (Springer, New York, 1986) p. 309.
[46] M.T. Saen's-Robles, M.D. Villela, G. Pucciarelli, F. Polo, M. Remacha, B.L. Ortiz, F.J. Vidales and J.P.G. Ballesta, Eur. J. Biochem. 177 (1988) 531.
[47] C. Casiano, A.T. Matheson and R.R. Traut, J. Biol. Chem. 265 (1990) 18757.
[48] A. Liljas and M.E. Newcomer, J. Mol. Biol. 153 (1982) 393.
[49] T. Arad, J. Piefke, S. Weinstein, H.S. Gewitz, A. Yonath and H.G. Wittmann, Biochimie 69 (1987) 1001.
[50] A. Yonath and Z. Berkovitch-Yellin, Curr. Opinion Struct. Biol. 3 (1993) 175.
[51] M. Eisenstein, B. Hardesty, O.W. Odom, W. Kudlicki, G. Kramer, T. Arad, F. Franceschi and A. Yonath, in: Biophysical Methods in Molecular Biology, Ed. G. Pifat (Balaban, 1994) p. 213.
[52] B. Hardesty, A. Yonath, G. Kramer, O.W. Odom, M. Eisenstein, F. Franceschi and W. Kudlicki, in: Membrane Protein Transport, Ed. S.S. Rothman (JAI, 1995) pp. 1, 77.
[53] A.J. Avila-Sakar, T.-L. Guan, T. Arad, M. F. Schmid, T.W. Loke, A. Yonath, J. Piefke, F. Franceschi and W. Chiu, J. Mol. Biol. 239 (1994) 689.
[54] H. Stark, F. Mueller, E. V. Orlova, M. Schatz, P. Dube, T. Erdemir, F. Zemlin, R. Brimacombe and M. van Heel, Structure 3 (1995) 815.
[55] J. Frank, J. Zhu, P. Penczek, Y. Li, S. Srivavtava, A. Verschoor, M. Rademacher, R. Grassuccl, R.K. Lata and R.K. Agarwal, Nature 376 (1995) 441.
[56] D. Beyer, E. Skripkin, J. Wadzack and K.H. Nierhaus, J. Biol. Chem. 269 (1994) 30713.